

State-dependent stiffness enhances wave propagation along elastic filaments

Clément Moreau,^{1,2,*} Benjamin J. Walker,^{3,4,†} Rebecca N. Poon,⁵ Daniel Soto,⁶ Daniel I. Goldman,⁶ Eamonn A. Gaffney,^{7,‡} and Kirsty Y. Wan^{5,§}

¹Nantes Université, École Centrale Nantes, CNRS, LS2N, UMR 6004, F-44000 Nantes, France

²Research Institute for Mathematical Sciences, Kyoto University, Kyoto, 606-8502, Japan

³Department of Mathematical Sciences, University of Bath, Bath, BA2 7AY, UK

⁴Department of Mathematics, University College London, London, WC1E 6BT, UK

⁵Living Systems Institute & Department of Mathematics and Statistics, University of Exeter, Exeter EX4 4QD, United Kingdom

⁶School of Physics, Georgia Institute of Technology, Atlanta, GA 30332, United States of America

⁷Mathematical Institute, University of Oxford, Oxford, OX2 6GG, United Kingdom

(Dated: February 22, 2024)

We study an elastic filament beating in a viscous fluid with curvature-dependent bending stiffness. Our numerical and experimental investigations reveal that such differential stiffness can sustain planar bending waves far along flexible filaments. In particular, basal actuation is a viable, parsimonious mechanism for generating high-amplitude planar bending waves, in stark contrast to the uniform-stiffness case. Further, the resulting beat patterns closely resemble the power-and-recovery strokes of propulsive biological filaments, suggesting applications in robotic and engineered systems.

INTRODUCTION

In a seminal study of the fluid-structure interactions of a swimming mammalian spermatozoon, Fig. 1a, in the 1950s Machin contrasted two popular competing hypotheses of the time [3]: (1) the tail-like flagellum is driven proximally (at its interface with the cell body) but is otherwise passive, and (2) the flagellum is driven by active elements along its length. Through a theoretical analysis of an idealised Euler elastica in the absence of inertia, Machin concluded that passive, proximally driven filaments were incapable of reproducing large-amplitude

bending waves that are characteristic of eukaryotic cilia and flagella [4–6]. In particular, Machin noted that, depending on parameters, one of two things occurred: (1) the amplitude of bending waves decayed rapidly along the flagellum, so that distal amplitudes were effectively negligible (Fig 3 F–J of [3]), or (2) bending only occurred with long wavelength, with fewer than approximately 1.5 wavelengths being present along the flagellum (Fig 3 A–E of [3]).

Machin’s study thereby effectively refuted the first of the two hypotheses for flagellar beating, a result later confirmed by experiments that culminated in the identification of dynein as the molecular motor responsible for force generation inside these filaments [7–9]. The cilium is now known to be a remarkably conserved organelle, found in almost all eukaryotes (Gibbons and Rowe [8], Mitchell [10], Lindemann [11], Merchant *et al.* [12] and Fig. 1). It is now well-established that ciliary beating is universally driven by distributed activity rather than localised actuation. Indeed, cilia completely isolated from the cell body continue to beat in the presence of ATP [13–15]. Hence, proximal actuation has been duly passed over as a driver of motility in eukaryotic systems. This notably contrasts with flagellated bacteria and archaea, which self-propel using a rotary motor that generates basal torque to spin a helical flagellum [16, 17].

However, looking beyond eukaryotes it is not clear that this neglect of proximal actuation as a viable mechanism for generating planar beating is justified or without loss. Natural systems often impose design limitations that guide and restrict theoretical study, whilst such constraints may no longer be applicable in engineered or synthetic systems [18–21]. For instance, while the material properties of biological flagella may be restricted by developmental or evolutionary constraints, engineered synthetic filaments may be designed with more freedom.

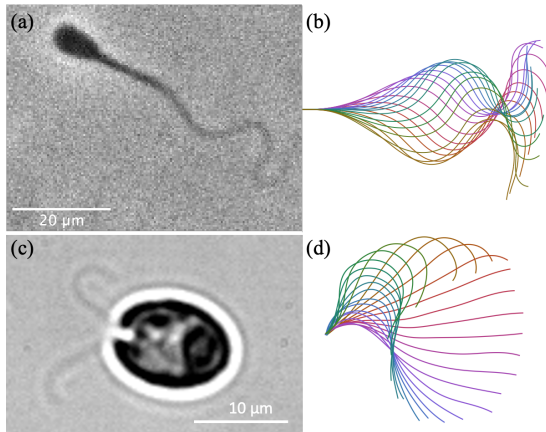


FIG. 1. Examples of flagellar actuation in biological microswimmers. Beating flagella of (a) a bovine spermatozoon and (c) *Chlamydomonas reinhardtii* display large amplitude bending at their distal ends. (b,d) Traces of the waveforms, color-coded in time, highlight the symmetric beat pattern for the sperm cell and marked asymmetry in *Chlamydomonas* between the power and recovery strokes. Images (a,b), (c,d) are reproduced with permission from Walker *et al.* [1] and Wan and Goldstein [2], respectively.

This raises a simple question: by modifying the mechanical properties of a filament, can the conclusions of Machin’s analysis be sidestepped? In other words, is it possible to produce realistic planar bending waves in engineered passive filaments for low-Reynolds number propulsion using only proximal actuation? If so, the simplicity of proximal actuation as a mechanism entails that circumventing Machin’s analysis would facilitate the development of markedly simple synthetic systems, such as novel bio-inspired devices for flow generation or underwater propulsion, without the need for intricate mechanisms of distributed driving or control. This could complement existing shape-based strategies for implementing directional compliance in terrestrial robotic appendages modelled upon the limbs of insects [22] or the undulatory motion of snakes [23].

Here, motivated by potential applications rather than biological propulsion mechanisms, we explore whether sustained bending waves along filaments immersed in a fluid can indeed be driven by basal actuation alone. More specifically, we consider a notion of state-dependent bending stiffness and explore the dynamics of filaments with this property, both theoretically and in a novel engineered physical system.

MACHIN’S LOW-AMPLITUDE MODEL

Machin [3] studied the propagation of bending waves along an elastic filament in a fluid using the dimensionless small-amplitude beam equation

$$\frac{\partial y}{\partial t} = -\frac{\partial^2}{\partial x^2} \left(E \frac{\partial^2 y}{\partial x^2} \right) \quad (1)$$

with boundary conditions

$$y(0, t) = 0, \quad \frac{\partial y}{\partial x}(0, t) = A \sin t, \quad (2a)$$

$$\frac{\partial^2 y}{\partial x^2}(1, t) = 0, \quad \frac{\partial^2 y}{\partial x^2}(1, t) = 0. \quad (2b)$$

This system corresponds to a filament with displacement y driven by rotation about a hinge at $x = 0$, with moment-free and shear-free conditions at the tip $x = 1$. Throughout, we use dimensionless quantities such that E captures the ratio of bending resistance to drag, the driving oscillations occur at unit frequency, and the filament is of unit length. Balancing terms in Eq. (1) gives rise to a natural dimensionless lengthscale $l = \sqrt[4]{E}$, over which planar elastic waves decay exponentially.

Many studies have significantly generalised Machin’s model, going far beyond the small-amplitude limit and into three dimensions [24–27], or have considered the effect of non-uniform, spatially-varying stiffness [28, 29]. Here, seeking an alternative generalisation, we incorporate state dependence into the stiffness, setting $E =$

$E(\frac{\partial^2 y}{\partial x^2})$ to depend on the local linearised curvature. For simplicity, we consider E to be piecewise constant, so that

$$E(\sigma) = \begin{cases} E_L & \text{if } \sigma > 0, \\ E_R & \text{if } \sigma \leq 0 \end{cases} \quad (3)$$

for unequal constants $E_L > E_R > 0$. Solving Eq. (1) is now somewhat involved, but we can estimate the appropriate decay lengthscale by considering a further simplification.

Suppose that, instantaneously, the filament is divided into two equal regions of positive and negative curvature, similar to a sinusoid over a single period. In the region of positive curvature, the appropriate decay lengthscale is $l_L = \sqrt[4]{E_L}$; in the region of negative curvature, the decay lengthscale is $l_R = \sqrt[4]{E_R}$. Note $l_L > l_R$. Hence, the amplitude of planar bending waves after passing through both regions experiences decay scaling with $\exp(-\frac{1}{2}[1/l_L + 1/l_R])$, as opposed to either of $\exp(-1/l_L)$ and $\exp(-1/l_R)$. Hence, there is an effective decay lengthscale of $2(1/l_L + 1/l_R)^{-1}$ in the filament, equal to the harmonic mean of the two individual lengthscales of decay. Notably, this is at least as large as the smallest lengthscale l_R , and approaches $2l_R$ as $E_L \rightarrow \infty$. Intuitively, this latter case corresponds to a filament that is extremely hard to bend in one direction, whilst being relatively compliant in the other.

This reasoning readily generalises to filaments where a proportion $\alpha \in (0, 1)$ is bent such that $E = E_R$. In this case, the effective lengthscale is $([1 - \alpha]/l_L + \alpha/l_R)^{-1}$, which approaches $l_R/\alpha > l_R$ as $E_L \rightarrow \infty$. Whilst clearly α should not be considered to be a fixed quantity in a dynamic filament, this back-of-the-envelope scaling analysis suggests that state-dependent bending stiffness could greatly enhance the effective decay length, with filaments thereby being able to transmit bending waves far along their lengths. Importantly, this mechanism unifies desirable properties of both high and low stiffness regimes: bending waves can be of high curvature (associated with the lower bending stiffness) and also propagate far along the filament (associated with the higher bending stiffness). Thus, filaments with differential stiffness are qualitatively different to their constant-stiffness counterparts.

To examine these idealised arguments thoroughly, a numerical study of filaments with differential bending stiffness is presented in Fig. 2, computed using FEniCS [30], wherein the state-dependent stiffness is taken to vary smoothly (but rapidly) between E_L and E_R (detailed in the Supplementary Material). We encourage readers to explore this system for themselves via a browser-based VisualPDE simulation [31]. The contrast between a uniform filament (a) and a filament with state-dependent stiffness (b) is marked, with the latter being highly asymmetric. The amplitude of distal motion is significantly greater in (b) than in (a), visible in the

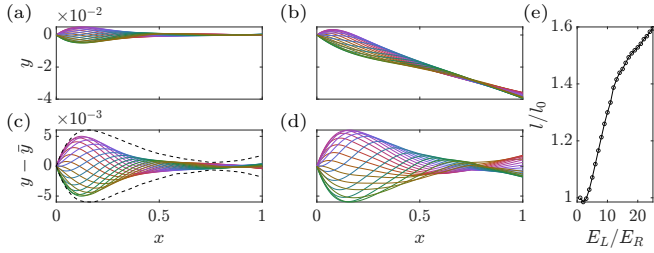


FIG. 2. Differential stiffness and small-amplitude beating. (a,b) Computed solutions of the small-amplitude beam equation over time with (a) $E_L = E_R = 10^{-4}$ and (b) $E_L = 10^{-3}$, $E_R = 10^{-4}$. (c,d) Deviation from the average configuration \bar{y} , highlighting increased amplitude with differential filament stiffness. The envelope of (d) is overlaid on (c) as black dashed curves. (e) Estimated decay lengthscale l as a function of differential stiffness, relative to the lengthscale l_0 in the equal-stiffness case. Here, $A = 0.1$.

mean-centered plots of (c) and (d). This enhancement of both the distal amplitude and the apparent decay lengthscale agree qualitatively with the scaling analysis. This is further supported by numerical estimation of the decay lengthscale as a function of the degree of differential stiffness (Fig. 2e), described in the Supplementary Material. Thus, at least in the small-amplitude regime, state-dependent stiffness is a plausible mechanism for propagating planar bending waves along filaments.

LARGE-AMPLITUDE BENDING

To investigate beyond the small-amplitude regime, we adopt a geometrically nonlinear framework [32, 33]. The analogue of Eq. (1) in the geometrically nonlinear regime is

$$E \frac{\partial \theta}{\partial s} + \int_s^1 [\mathbf{x}(\tilde{s}) - \mathbf{x}(s)] \times \mathbf{f}(\tilde{s}) d\tilde{s} = 0 \quad (4)$$

written in terms of the tangent angle θ (measured relative to a fixed axis), position $\mathbf{x} = (x, y)$, and hydrodynamic drag \mathbf{f} , each functions of arclength $s \in [0, 1]$ and dimensionless. The derivation of this integral equation and the underlying assumptions are described in detail by Moreau *et al.* [32], recounted in part in the Supplementary Material. In the nonlinear regime, curvature is $\kappa = \frac{\partial \theta}{\partial s}$, so that $E = E(\kappa)$. Solving this integro-differential equation numerically (as described in the Supplementary Material) allows us to test the predictions of the linear theory well beyond its regime of validity. In the following, we set $A = \pi/2$.

In this general regime, a quantitative measure of the effects of stiffness is the relative increase in maximum curvature over one beating period, averaged over the flag-

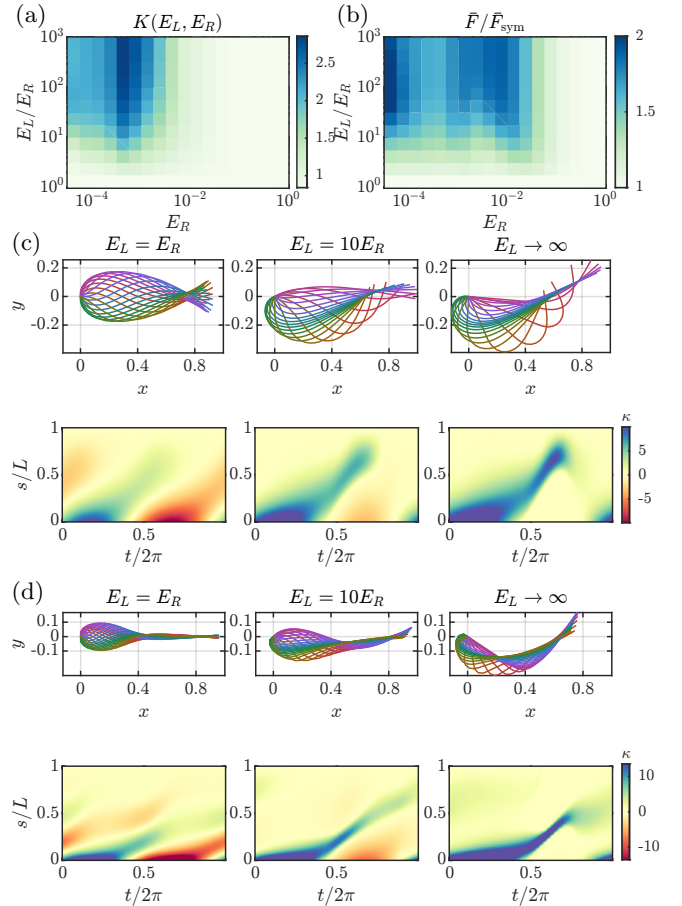


FIG. 3. Effects of differential stiffness in the geometrically nonlinear regime ($A = \pi/2$), obtained from numerical solution of Eq. (4). (a,b) Relative increase in (a) maximal curvature and (b) average force at the pinned end, for a range of stiffnesses E_R and differential stiffnesses E_L/E_R . Example waveforms are shown below for (c) medium stiffness ($E_R = 1.6 \times 10^{-3}$) and (d) low stiffness ($E_R = 1 \times 10^{-4}$). (c,d) Example beating patterns (rotated in the beating plane to align horizontally) and associated curvature kymographs for filaments of (c) medium stiffness ($E_R = 1.6 \times 10^{-3}$) and (d) low stiffness ($E_R = 1 \times 10^{-4}$). From left to right: symmetric beating ($E_L = E_R$), resembling the classical solution of Fig. 2; an intermediate case ($E_L/E_R = 10$), matching that studied in the small-amplitude regime; and a highly asymmetric “locking” case ($E_L/E_R = 10^3$), effectively forbidding negative curvatures.

ellum, defined for given E_L and E_R as

$$K(E_L, E_R) = \int_0^1 \frac{\max_t |\kappa_{E_L, E_R}(s, t)|}{\max_t |\kappa_{E_R, E_R}(s, t)|} ds, \quad (5)$$

where the maximum over t is computed over one time period in the limiting periodic regime. Naturally, $\kappa_{E_L, E_R}(s, t)$ and $\kappa_{E_R, E_R}(s, t)$ refer to the curvature for the asymmetric and symmetric filaments, respectively.

This quantity is presented in panel (a) of Fig. 3, plotted as a function of E_R and the differential stiffness E_L/E_R , demonstrating that differential stiffness can greatly en-

hance the curvatures attained by a filament during a beating period. The relative increase is three-fold around $E_R \approx 1 \times 10^{-3}$.

To confirm that the increase in average curvature is localised towards the distal end of the filament, we also determined the maximum value K_{\max} and its argument s_{\max} over $s \in [0, 1]$ of the integrand in Eq. (5), indicating where the qualitative change between uniform and differential stiffness is the greatest. For any value of E_L and E_R , s_{\max} takes values between 0.5 and 0.8, confirming the trend in Fig. 3. Around $E_R \approx 1 \times 10^{-3}$, the corresponding value of K_{\max} goes up to 6, further highlighting the capacity of differential stiffness to transport and even amplify curvature for large beating amplitudes.

Machin identified (in the small-amplitude limit) that exponential decay significantly hinders planar wave propagation towards the distal end when the filament length exceeds five times the characteristic lengthscale $\sqrt[4]{E_R}$. Surprisingly, the parameter regime in which we see maximal curvature increase due to differential stiffness approximately corresponds to this case. Moreover, the curvature increase remains markedly high even when considering very small E_R ($< 10^{-4}$, representing a filament more than 10 times longer than the relaxation lengthscale), for which the effect of proximal actuation with uniform stiffness is virtually negligible at the distal end.

Figure 3b displays the magnitude \bar{F} of the pinning force, exerted on the point of attachment at the proximal end, averaged over one beating period, and normalised by the time-averaged force without differential stiffness, \bar{F}_{sym} . As should be expected, maintaining a prescribed actuation while increasing filament stiffness for positive curvature comes at the cost of increasing the average pinning force. However, this relative increase remains smaller than the relative curvature enhancement through most values of E_R and E_L , indicating that differential stiffness constitutes an efficient way of increasing curvature according to this measure. For all values of E_L/E_R , the relative force $\bar{F}/\bar{F}_{\text{sym}}$ has a local minimum with respect to E_R for $E_R \approx 1.6 \times 10^{-3}$. Simultaneously, $K(E_L, E_R)$ is approximately maximal, so that the ratio between $K(E_L, E_R)$ and $\bar{F}/\bar{F}_{\text{sym}}$ is also approximately maximal. This value of E_R appears to be optimal for enhanced curvature generation with differential stiffness.

Panels (c) and (d) of Fig. 3 illustrate filament beats in the large amplitude regime for various degrees of differential stiffness. In the left column, we take $E_L = E_R$ and reproduce the symmetric, short-lengthscale beating predicted by Machin’s low-amplitude analysis for differing baseline stiffness E_R . In the subsequent columns, increasing degrees of differential stiffness yield larger amplitude deviations at the distal end of the filament while also allowing for high-curvature planar bending waves to propagate. These beats are further represented in the plots of signed curvature κ beneath the beating patterns, from which the high curvatures of the asymmetric regimes are

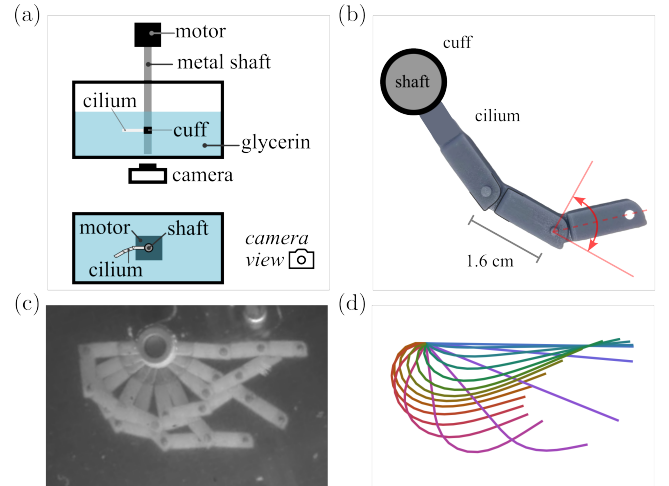


FIG. 4. Experimental realisation of differential stiffness in a bio-inspired macroscale robotic cilium. Motion is driven only by actuating the base of the filament. (a) Diagram of the experimental setup, not to scale. The cilium is placed in a tank of glycerin, and imaged from below. The cilium is connected to the driving motor by a vertical metal shaft. (b) Detail of the locking mechanism. The links are designed so that each link can rotate freely only within the 90° angle indicated in red. (c) Snapshots of the robotic filament overlaid in time compared to (d) a simulated waveform, with $A = \pi/2$, $E_R = 2 \times 10^{-3}$, $E_L \gg E_R$ highlighting marked agreement between the synthetic and *in silico* systems.

evident. The spatial extent of bending waves is also clearly visible, with differential stiffness giving rise to far-reaching bending. Moreover, in the case $E_R \approx 1.6 \times 10^{-3}$ (Fig. 3c), the resulting beat patterns begin to resemble the *power-and-recovery strokes* typical of most cilia, including *Chlamydomonas* (Fig. 1d), other protists [34–36], and vertebrate respiratory cilia [37].

Thus, even beyond the small-amplitude regime, differential stiffness presents itself as an efficient mechanism for enhancing elastic planar wave propagation.

ENGINEERING BIOMIMETIC BEATING

Given the striking resemblance of the simulated beat of Fig. 3c with those seen in certain biological specimens, can we realise biomimetic beating in practice with a simple physical model, using only basal actuation and differential stiffness? To explore this, we built a macroscopic robotic realisation of a basally actuated filament, schematised in Fig. 4a. The continuum limit is difficult to implement, so our robotic filament comprises a finite number of links connected by custom hinges that are designed to qualitatively mimic differential stiffness [18].

These hinges, illustrated in Fig. 4b, are asymmetric in shape, so they only admit bending in one direction, similar to the “locking” limit $E_L \gg E_R$ explored above.

Each of the three links is 1.6 cm long, with a 1.2 cm basal attachment, so that the total length of the filament from its rotation point is 6 cm. The locking hinges are designed to reproduce the most extreme case of differential stiffness in the limit of $E_L \gg E_R$ (as seen in Fig. 3c).

The filament is driven at the base by a XL430-W250 dynamixel motor, which rotates through 180° at an angular velocity of 5° s^{-1} . To remain in the low-Reynolds regime, the filament is placed in a tank of glycerin, which has density of $1.26 \times 10^3 \text{ kg m}^{-3}$ and viscosity 1.4 Pa.s. The oscillatory Reynolds number $\rho f L^2 / \eta = 0.03$. Visual inspection of the beating filament confirmed that inertial coasting was negligible. The tank measures 60 cm by 32 cm, with depth 18 cm. The filament is positioned far from walls to minimise boundary interactions. Imaging was performed at 1 Hz using a Logitech webcam. The cilia were resin printed using an Anycubic Photon Mono X, in Anycubic resin, and density matched to the glycerin.

Prescribing a basal amplitude $A = \pi/2$, the beat pattern of the robotic filament is showcased in Fig. 4c. Even without elasticity, the power and recovery strokes are clearly distinguished, with experimental waveforms closely resembling the cilia-like beating observed in our nonlinear simulations (Fig. 4d). A full and faithful model of the robotic system and a complete parameter analysis will be explored in future study.

SUMMARY AND CONCLUSIONS

We have demonstrated that enhanced wave propagation in passive filaments driven at one end can be realised with state-dependent bending stiffness. Our results are underpinned by both numerical investigation and theoretical arguments, and extensively extend Machin's 1950s analysis [3] of sea urchin flagellar beating. In particular, we have demonstrated how curvature dependent stiffness, realised by a differing stiffnesses for the direction of bending, can pragmatically sidestep the conclusions of Machin's study [3] to generate biologically realistic planar waveforms using basal actuation alone. This highlights and establishes the ready potential for simple, parsimonious synthetic systems to reproduce this well-studied and widely conserved biological phenomenon.

Furthermore, dynamic structural heterogeneities and asymmetries harboured within the ciliary axoneme have the prospect of contributing to an effective state-dependent stiffness [38–41]. Thus the investigation of asymmetric, state-dependent stiffness has a role in further elucidating the mechanics of eukaryotic flagellar and ciliary beating and, more generally, paves the way for new avenues of multidisciplinary enquiry into the motility and actuation of synthetic systems at the microscale.

ACKNOWLEDGEMENTS

This work was funded by the Japan Society for the Promotion of Science (Fellowship No. PE22023 and Grant No. 22KF0197 to C.M) and the Research Institute for Mathematical Sciences, an International Joint Usage/Research Center located at Kyoto University (C.M), by the Royal Commission for the Exhibition of 1851 (B.J.W), by the European Research Council under the European Union's Horizon 2020 research and innovation programme grant 853560 EvoMotion (K.Y.W), and a Company of Biologists travelling fellowship (R.N.P and K.Y.W).

* clement.moreau@cnrs.fr

† bjw43@bath.ac.uk

‡ gaffney@maths.ox.ac.uk

§ k.y.wan2@exeter.ac.uk

- [1] B. J. Walker, S. Phuyal, K. Ishimoto, C.-k. Tung, and E. A. Gaffney, Computer-assisted beat-pattern analysis and the flagellar waveforms of bovine spermatozoa, *Royal Society Open Science* **7**, 200769 (2020).
- [2] K. Y. Wan and R. E. Goldstein, Rhythmicity, recurrence, and recovery of flagellar beating, *Physical Review Letters* **113** (2014).
- [3] K. E. Machin, Wave propagation along flagella, *J. Exp. Biol.* **35**, 796 (1958).
- [4] C. Brennen and H. Winet, Fluid-mechanics of propulsion by cilia and flagella, *Ann. Rev. Fluid Mech.* **9**, 339 (1977).
- [5] D. M. Woolley and G. G. Vernon, A study of helical and planar waves on sea urchin sperm flagella, with a theory of how they are generated, *J. Exp. Biol.* **204**, 1333 (2001).
- [6] M. T. Gallagher, G. Cupples, E. H. Ooi, J. Kirkman-Brown, and D. Smith, Rapid sperm capture: high-throughput flagellar waveform analysis, *Human Reproduction* **34**, 1173 (2019).
- [7] I. Gibbons, Studies on protein components of cilia from tetrahymena pyriformis, *PNAS* **50**, 1002 (1963).
- [8] I. Gibbons and A. Rowe, Dynein - a protein with adenosine triphosphatase activity from cilia, *SCIENCE* **149**, 424 (1965).
- [9] K. E. Summers and I. R. Gibbons, Adenosine triphosphate-induced sliding of tubules in trypsin-treated flagella of sea-urchin sperm, *PNAS* **68**, 3092 (1971).
- [10] D. R. Mitchell, Evolution of cilia, *Cold Spring Harbor Perspectives in Biology* **9**, a028290 (2017).
- [11] C. B. Lindemann, The flagellar germ-line hypothesis: How flagellate and ciliate gametes significantly shaped the evolution of organismal complexity, *Bioessays* **44**, 10.1002/bies.202100143 (2022).
- [12] S. S. Merchant, S. E. Prochnik, O. Vallon, E. H. Harris, S. J. Karpowicz, G. B. Witman, A. Terry, A. Salamov, L. K. Fritz-Laylin, L. Marechal-Drouard, W. F. Marshall, L.-H. Qu, D. R. Nelson, A. A. Sanderfoot, M. H. Spalding, V. V. Kapitonov, Q. Ren, P. Ferris, E. Lindquist, H. Shapiro, S. M. Lucas, J. Grimwood, J. Schmutz, C. A. Team, I. V. JGI Annotation Team Grigoriev, D. S. Rokhsar, and A. R. Grossman, The chlamydomonas

- genome reveals the evolution of key animal and plant functions, *Science* **318**, 245 (2007).
- [13] V. F. Geyer, J. Howard, and P. Sartori, Ciliary beating patterns map onto a low-dimensional behavioural space, *Nature Physics* **18**, 332 (2022).
- [14] M. Bessen, R. B. Fay, and G. B. Witman, Calcium control of waveform in isolated flagellar axonemes of *Chlamydomonas*, *The Journal of Cell Biology* **86**, 446 (1980).
- [15] K. Y. Wan, The beat of isolated cilia, *Nature Physics* **18**, 234 (2022).
- [16] H. C. Berg and R. A. Anderson, Bacteria swim by rotating their flagellar filaments, *Nature* **245**, 380 (1973).
- [17] M. Beeby, J. L. Ferreira, P. Tripp, S.-V. Albers, and D. R. Mitchell, Propulsive nanomachines: the convergent evolution of archaella, flagella and cilia, *FEMS microbiology reviews* **44**, 253 (2020).
- [18] K. Diaz, T. L. Robinson, Y. O. Aydin, E. Aydin, D. I. Goldman, and K. Y. Wan, A minimal robophysical model of quadriflagellate self-propulsion, *Bioinspiration & Biomimetics* **16**, 066001 (2021).
- [19] T. ul Islam, Y. Wang, I. Aggarwal, Z. Cui, H. Es-lami Amirabadi, H. Garg, R. Kooi, B. B. Venkataramanachar, T. Wang, S. Zhang, P. R. Onck, and J. M. J. den Toonder, Microscopic artificial cilia – a review, *Lab Chip* **22**, 1650 (2022).
- [20] S. Sareh, J. Rossiter, A. Conn, K. Drescher, and R. E. Goldstein, Swimming like algae: biomimetic soft artificial cilia, *Journal of the Royal Society Interface* **10**, 20120666 (2013).
- [21] S. Lim, Y. Du, Y. Lee, S. K. Panda, D. Tong, and M. Khalid Jawed, Fabrication, control, and modeling of robots inspired by flagella and cilia, *Bioinspiration & Biomimetics* **18**, 011003 (2023).
- [22] J. C. Spagna, D. I. Goldman, P.-C. Lin, D. E. Koditschek, and R. J. Full, Distributed mechanical feedback in arthropods and robots simplifies control of rapid running on challenging terrain, *Bioinspiration & biomimetics* **2**, 9 (2007).
- [23] T. Wang, J. Whitman, M. Travers, and H. Choset, Directional compliance in obstacle-aided navigation for snake robots, in *2020 American Control Conference (ACC) (IEEE, 2020)* pp. 2458–2463.
- [24] C. J. Brokaw, Effects of increased viscosity on the movements of some invertebrate spermatozoa, *J. Exp. Biol.* **45**, 113 (1966).
- [25] M. Hines and J. J. Blum, Bend propagation in flagella I. Derivation of equations of motion and their simulation, *Biophys. J.* **23**, 41 (1978).
- [26] S. Camalet and F. Julicher, Generic aspects of axonemal beating, *New J. Phys.* **2**, 24.1 (2000).
- [27] B. Rallabandi, Q. Wang, and M. Potomkin, Self-sustained three-dimensional beating of a model eukaryotic flagellum, *Soft Matter* **18**, 5312 (2022).
- [28] Z. Peng, G. J. Elfring, and O. S. Pak, Maximizing propulsive thrust of a driven filament at low Reynolds number via variable flexibility, *Soft Matter* **13**, 2339 (2017).
- [29] C. V. Neal, A. L. Hall-McNair, J. Kirkman-Brown, D. J. Smith, and M. T. Gallagher, Doing more with less: The flagellar end piece enhances the propulsive effectiveness of human spermatozoa, *Phys. Rev. Fluids* **5**, 073101 (2020).
- [30] A. Logg, K.-A. Mardal, and G. Wells, eds., *Automated Solution of Differential Equations by the Finite Element Method*, Lecture Notes in Computational Science and Engineering, Vol. 84 (Springer Berlin Heidelberg, Berlin, Heidelberg, 2012).
- [31] B. J. Walker, A. K. Townsend, A. K. Chudasama, and A. L. Krause, VisualPDE: rapid interactive simulations of partial differential equations, *Bulletin of Mathematical Biology* **85**, 113 (2023).
- [32] C. Moreau, L. Giraldo, and H. Gadêlha, The asymptotic coarse-graining formulation of slender-rods, bio-filaments and flagella, *Journal of The Royal Society Interface* **15**, 20180235 (2018).
- [33] B. J. Walker, K. Ishimoto, H. Gadelha, and E. A. Gaffney, Filament mechanics in a half-space via regularised Stokeslet segments, *J. Fluid. Mech.* **879**, 808 (2019).
- [34] Z. Wang, T. Beneke, E. Gluenz, and R. J. Wheeler, The single flagellum of *Leishmania* has a fixed polarisation of its asymmetric beat, *Journal of Cell Science* **133**, jcs246637 (2020).
- [35] M. A. Sleight, Ciliary propulsion in protozoa, *Science Progress (1933-)* **73**, 317 (1989).
- [36] H. Laeverenz-Schlogelhofer and K. Y. Wan, Bioelectric control of locomotor gaits in the walking ciliate *Euplotes*, *Current Biology* (2024).
- [37] M. J. Sanderson and M. A. Sleight, Ciliary activity of cultured rabbit tracheal epithelium: beat pattern and metachrony, *Journal of Cell Science* **47**, 331 (1981).
- [38] K. H. Bui, T. Yagi, R. Yamamoto, R. Kamiya, and T. Ishikawa, Polarity and asymmetry in the arrangement of dynein and related structures in the *Chlamydomonas* axoneme, *Journal of Cell Biology* **198**, 913 (2012).
- [39] S. K. Dutcher, Asymmetries in the cilia of *Chlamydomonas*, *Philosophical Transactions of the Royal Society B* **375**, 20190153 (2020).
- [40] Z. Chen, G. A. Greenan, M. Shiozaki, Y. Liu, W. M. Skinner, X. Zhao, S. Zhao, R. Yan, Z. Yu, P. V. Lishko, *et al.*, In situ cryo-electron tomography reveals the asymmetric architecture of mammalian sperm axonemes, *Nature Structural & Molecular Biology* **30**, 360 (2023).
- [41] J. Lin and D. Nicastro, Asymmetric distribution and spatial switching of dynein activity generates ciliary motility, *Science* **360**, eaar1968 (2018), <https://www.science.org/doi/pdf/10.1126/science.aar1968>.